Icarus 248 (2015) 424–447

Contents lists available at ScienceDirect

Icarus

journal homepage: www.elsevier.com/locate/icarus

Lunar floor-fractured craters as magmatic intrusions: Geometry, modes of emplacement, associated tectonic and volcanic features, and implications for gravity anomalies

Lauren M. Jozwiak [a,*], James W. Head [a], Lionel Wilson [b]

[a] Department of Geological Sciences, Brown University, Providence, RI 02912, USA
[b] Lancaster Environment Centre, Lancaster University, Lancaster LA1 4YQ, UK

ARTICLE INFO

Article history:
Received 29 May 2014
Revised 8 October 2014
Accepted 12 October 2014
Available online 15 November 2014

Keywords:
Volcanism
Moon, interior
Moon, surface

ABSTRACT

Lunar floor-fractured craters are a class of 170 lunar craters with anomalously shallow, fractured floors. Two end-member processes have been proposed for the floor formation: viscous relaxation, and subcrater magmatic intrusion and sill formation. Recent morphometric analysis with new Lunar Reconnaissance Orbiter Laser Altimeter (LOLA) and image (LROC) data supports an origin related to shallow magmatic intrusion and uplift. We find that the distribution and characteristics of the FFC population correlates strongly with crustal thickness and the predicted frequency distribution of overpressurization values of magmatic dikes. For a typical nearside lunar crustal thickness, dikes with high overpressurization values favor surface effusive eruptions, medium values favor intrusion and sill formation, and low values favor formation of solidified dikes concentrated lower in the crust. We develop a model for this process, make predictions for the morphologic, morphometric, volcanic, and geophysical consequences of the process and then compare these predictions with the population of observed floor-fractured craters. In our model, the process of magmatic intrusion and sill formation begins when a dike propagates vertically towards the surface; as the dike encounters the underdense brecciated region beneath the crater, the magmatic driving pressure is insufficient to continue vertical propagation, but pressure in the stalled dike exceeds the local lithostatic pressure. The dike then begins to propagate laterally forming a sill which does not propagate past the crater floor region because increased overburden pressure from the crater wall and rim crest pinch off the dike at this boundary; the sill then continues to inflate, further raising and fracturing the brittle crater floor. When the intrusion diameter to intrusion depth ratio is smaller than a critical value, the intrusion assumes a laccolith shape with a domed central region. When the ratio exceeds a critical value, the intrusion concentrates bending primarily at the periphery, resulting in a flat, tabular intrusion. We predict that this process will result in concentric fractures over the region of greatest bending. This location is close to the crater wall in large, flat-floored craters, as observed in the crater Humboldt, and interior to the crater over the domed floor in smaller craters, as observed in the crater Vitello. A variety of volcanic features are predicted to be associated with the solidification and degassing of the intrusion; these include: (1) surface lava flows associated with concentric fractures (e.g., in the crater Humboldt); (2) vents with no associated pyroclastic material, from the deflation of under-pressurized magmatic foam (e.g., the crater Damoiseau); and (3) vents with associated pyroclastic deposits from vulcanian eruptions of highly pressurized magmatic foam (e.g., the crater Alphonsus). The intrusion of basaltic magma beneath the crater is predicted to contribute a positive component to the Bouguer gravity anomaly; we assess the predicted Bouguer anomalies associated with FFCs and outline a process for their future interpretation. We conclude that our proposed mechanism serves as a viable formation process for FFCs and accurately predicts numerous morphologic, morphometric, and geophysical features associated with FFCs. These predictions can be further tested using GRAIL (Gravity Recovery and Interior Laboratory) data.

* Corresponding author.
E-mail address: lauren_jozwiak@brown.edu (L.M. Jozwiak).

http://dx.doi.org/10.1016/j.icarus.2014.10.052
0019-1035/

1. Introduction

Floor-fractured craters (FFCs) are a class of 170 lunar craters characterized by their anomalously shallow, fracture-covered floors. First described in detail by Schultz (1976) with initial mapping of >80 FFCs by Wilhelms (1987), these craters are divided into eight morphologic subclasses (Schultz, 1976; Jozwiak et al., 2012). Each subclass possesses distinct morphologic characteristics, including features such as mare deposits, moat features, dark halo deposits, either convex-up or flat-floor profiles, and predominately radial, concentric, or polygonal fracture features.

There are two proposed formation mechanisms for floor-fractured craters (FFCs): (1) viscous relaxation, wherein the crater floor rebounds to fill the crater at a rate controlled by the subsurface viscosity structure resulting in an overall amplitude shallowing of long-wavelength crater topography (Masursky, 1964; Daneš, 1965; Cathles, 1975; Hall et al., 1981; Dombard and Gillis, 2001), and (2) magmatic intrusion and sill formation, wherein a dike propagates from the mantle, stalls beneath the crater, then spreads laterally beneath the crater and inflates, forming a laccolith and lifting up and fracturing the overlying crater floor (Brennan, 1975; Schultz, 1976; Wichman and Schultz, 1996; Jozwiak et al., 2012).

Jozwiak et al. (2012) analyzed the morphology of 170 FFCs using new Lunar Orbiter Laser Altimeter (LOLA) data and Lunar Reconnaissance Orbiter Camera (LROC) images to assess support for each of the proposed formation mechanisms. They found no direct support for FFC formation via viscous relaxation; they did, however, find morphologic support for FFC formation as a result of magmatic intrusion and sill formation. The lines of evidence favoring magmatic intrusion as the formation mechanism included the large amount of floor shallowing, the unaltered crater rim crest height, the lack of crater symmetry, moat features, the location of FFCs away from basin edges where no basin-related thermal anomalies are expected, and the significant population of FFCs with diameters less than 30 km, a diameter range not favored for viscous relaxation (see Jozwiak et al., 2012).

Significant increases in our knowledge of FFCs from LOLA data are high-resolution topography and detailed profiles of the crater floor, permitting morphometric analysis of crater depth, shape and volume, and analysis of floor-fracture structure. In contrast to fresh craters with concave-down floor profiles (such as Tycho; Fig. 1a), FFCs predominately display either flat or slightly upbowed floor profiles (such as displayed by Humboldt; Fig. 1b), or convex-up floor profiles (as displayed by the smaller, Bohnenberger crater; Fig. 1c). Models of viscous relaxation predict that this process will result in a shallower, gently upbowed floor (Hall et al., 1981; Dombard and Gillis, 2001; Fig. 1d), inconsistent with both the observed broadly flat to slightly upbowed floor profiles (Fig. 1b) and the strongly upbowed floor profiles (Fig. 1c). On the other hand, these observed profiles (Fig. 1b and c) might be explained as different manifestations of a magmatic intrusion process, arising from different laccolith morphologies, a hypothesis that we investigate in Section 3.

Based on the morphologic and morphometric support for magmatic intrusion as the formation mechanism for FFCs (e.g. Schultz,

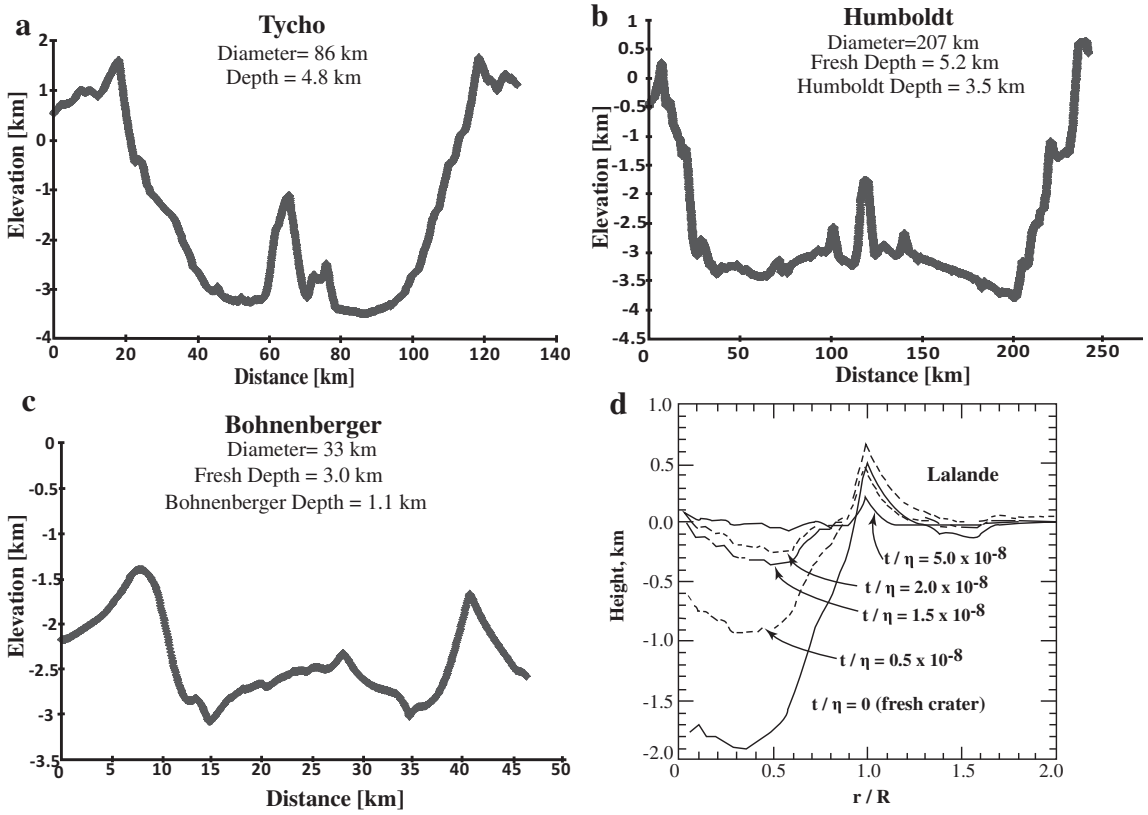

Fig. 1. Comparison of crater floor profiles including: (a) the fresh, unmodified crater Tycho (43.3°S, 11.3°W), with a concave-down floor profile, (b) the large floor-fractured crater Humboldt (27.2°S, 80.9°E), with a gently upbowed and shallowed floor profile, (c) the small floor-fractured crater Bohnenberger (16.2°S, 40.0°E), with a highly domed crater floor region separated from the crater wall by a distinct "v"-shaped trough, and (d) a model of a viscously relaxed crater from Hall et al. (1981). The topographic profiles for (a, b, and c) are shown using LOLA 512 px/deg gridded data. The given crater depths for (a, b, and c) were measured from LOLA topography, and the fresh depths were calculated according to Pike (1980). (d) This half-space model of a viscously relaxed crater floor illustrates the exceedingly high thermal gradients (interpreted from the characteristic viscous relaxation time τ/η) required to achieve a crater floor profile similar to profiles observed in craters Humboldt and Bohnenberger.